Distortion of Rabi oscillations in a compact cold-atom clock

Xinchuan Ouyang,[1,2] Bowen Yang,[1,2] Qingqing Hu,[3] Hanghang Qi,[1,2] Ling Xiao,[1] Jinyin Wan,[1,*] and Huadong Cheng[1,2,†]

[1]*Key Laboratory of Quantum Optics and Center of Cold Atom Physics, Shanghai Institute of Optics and Fine Mechanics, Chinese Academy of Sciences, Shanghai 201800, China*

[2]*Center of Materials Science and Optoelectronics Engineering, University of Chinese Academy of Sciences, Beijing 100049, China*

[3]*Advanced Interdisciplinary Technology Research Center, National Innovation Institute of Defense Technology, Beijing 100010, China*

(Received 17 December 2020; revised 26 February 2021; accepted 7 April 2021; published 26 April 2021)

We report on experimental measurements and theoretical calculations of Rabi oscillation distortion during rubidium clock transition in a compact cold-atom clock. The distortion of the Rabi oscillations of the clock transition caused by the magnetically sensitive transitions between magnetic sublevels is related to the duration and amplitude of the microwave pulse, the density distribution of cold atoms, and the biased magnetic field inside the microwave cavity. The theoretical calculations agreed well with the experimental results. The Rabi oscillation measurements are beneficial for determining the optimal parameters of a cold-atom clock and identifying the uniformity of the microwave field inside the cavity. This measurement can be extended to the atomic fountain clock and the vapor-cell atomic clock.

DOI: 10.1103/PhysRevA.103.043118

I. INTRODUCTION

A two-level quantum system interacting resonantly with a coherent external field is significant for atomic and quantum physics [1–3]. The coherence lifetimes of these quantum systems can be determined by coherent population oscillations [4], namely, Rabi oscillations, which are typically observed in an atomic clock [5–8], a quantum dot [9,10], Josephson junction qubits [11], and Rydberg states [12]. In the case of an atomic clock using a microwave cavity, Rabi oscillations and Ramsey fringes are measured to determine the lock loop parameters [13,14]. The shape, contrast, and signal-to-noise ratio of the Rabi and Ramsey signals are critical for the performance of an atomic clock. The factors that affect the clock transition of the atomic fountain primary frequency standard have been extensively studied [15,16]. However, only a few studies have concentrated on the compact cold-atom clock [17,18].

In the last 20 years, laser cooling of neutral atoms with an isotropic light [19–21] has gained great attention from researchers due to its simple system structure, all-optical scheme, and larger cooling efficiency than optical molasses. Especially, this cooling scheme can be used to develop the compact cold-atom clock, which has great potential used in space [18,22,23]. In this paper, we demonstrate a Rabi oscillation measurement of the clock transition of the integrating-sphere cold-atom clock (ISCAC), which is different from the typical Rabi oscillations of two-level atoms resonantly interacting with a coherent external field and exhibits complex features. We theoretically analyze the influence of the inhomogeneity of microwave magnetic fields, the density distribution of the cold atoms, and the duration and amplitude of the microwave pulse on the Rabi oscillations. Finally, we provide an explanation for this Rabi oscillation distortion, which can provide an important reference for designing the high-performance on-board cold-atom clock, and the theory can also be extended to other types of microwave clock, such as atomic fountain and vapor-cell clocks.

II. EXPERIMENTAL SCHEME AND THEORY

A schematic of the experiment setup is shown in Fig. 1(a). The microwave cavity is placed in a vacuum chamber, with a resonance frequency corresponding to the ground-state hyperfine transition frequency of ^{87}Rb (6.834 GHz). The biased magnetic field generated by the coil provides a quantization axis. The physical package is placed within a five-layer magnetic shield to minimize the effect from the external magnetic field. The cooling, repumping, and pumping lights are injected into the microwave cavity through four multimode fibers and reflected by the inner surface of the cavity to produce the diffuse light [17]. The probe beam is retroreflected through the physical package by a top mirror and passed through the quarter-wave plate, finally reflected by the polarizing beam splitter into the photodetector.

The time sequence of the experiment is shown in Fig. 1(b). After the cooling phase, the cold atoms ($\sim$30 μK [24]) populate in the states $|F = 2, m_F = 0, \pm1, \pm2\rangle$. Subsequently, the atoms are prepared into the states $|F = 1, m_F = 0, \pm1\rangle$ by the pumping light. Next, the atoms in the state $|1, 0\rangle$ (representing $|F = 1, m_F = 0\rangle$, the same as below) are pumped into the state $|2, 0\rangle$ by a resonance microwave pulse with duration τ. Finally, the number of atoms in the state $|F = 2\rangle$ is detected with a resonant probe light. For absorption detection, the

*jywan@siom.ac.cn
†chenghd@siom.ac.cn

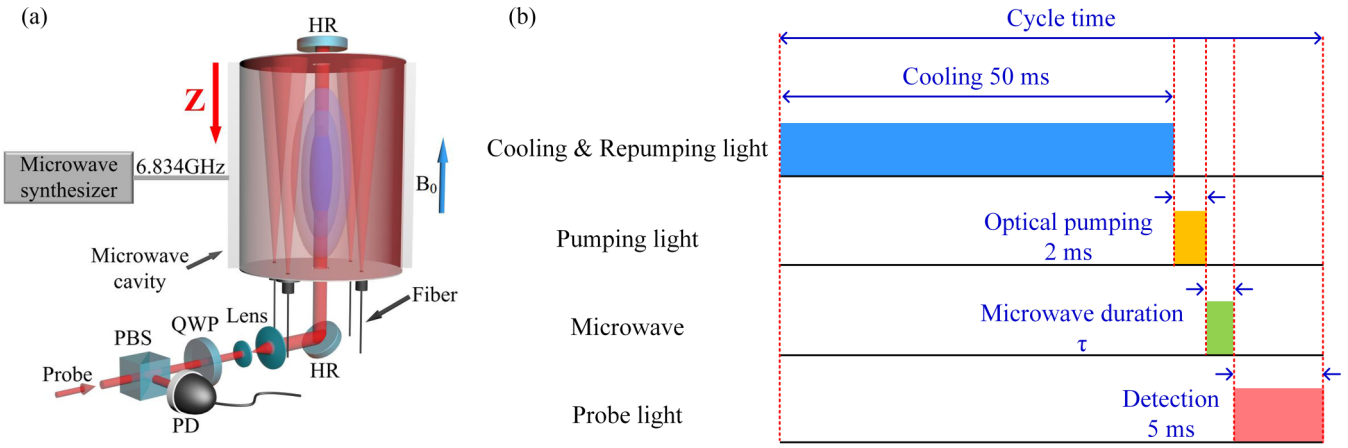

FIG. 1. (a) Schematic of the experimental setup. HR, highly reflective mirror; PBS, polarizing beam splitter; PD, photodetector; QWP, quarter-wave plate. (b) Time sequence of the experiment.

number of cold atoms in the state $|F = 2\rangle$ can be estimated with the following equation [25]:

$$N = \frac{\pi a^2}{\sigma_0}\left[\frac{I_0 - I_t}{I_s} + \left(\frac{4\delta^2}{K^2} + 1\right)\ln\left(\frac{I_0}{I_t}\right)\right], \tag{1}$$

where a is the radius of the probe beam and σ_0 is the resonant cross-sectional area. The inner space of microwave cavity is filled with cold atoms after the cooling phase. The beam diameter of the probe light is smaller than that of the cold-atom cloud. I_0 and I_t represent the probe light intensity across the beam before and after going through the physical package, respectively. Moreover, δ is the probe light detuning from the resonance frequency of $|F = 2\rangle$ to $|F' = 3\rangle$, K is the natural linewidth of the ^{87}Rb D_2 line transition, and I_s is the on-resonance saturation intensity. The theoretical model is presented below. Here, only the transitions between sublevels of the hyperfine ground states were considered, as shown in Fig. 2. We assume that the microwave magnetic field driving the transitions between $|F = 1, m_F = 0, \pm 1\rangle$ and $|F = 2, m_F = 0, \pm 1\rangle$ is parallel to the biased magnetic field. The Hamiltonian describing the hyperfine structure and the atomic interaction with external magnetic field **B** for the ground state of ^{87}Rb is

$$\mathrm{H} = \frac{\mathrm{A_{hfs}}}{\hbar^2}\mathbf{I}\cdot\mathbf{S} + \frac{\mu_B}{\hbar}(g_S\mathbf{S} + g_I\mathbf{I})\cdot\mathbf{B}, \tag{2}$$

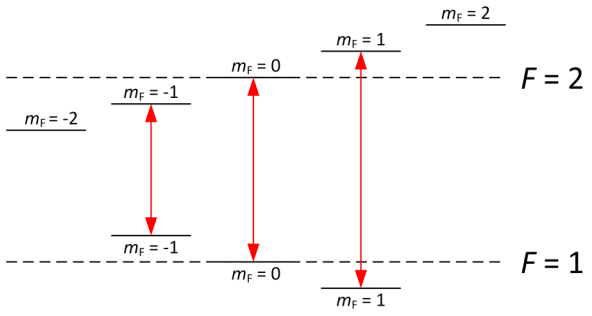

FIG. 2. Energy levels of the hyperfine state of the ^{87}Rb atom.

where $\mathrm{A_{hfs}}$ is the magnetic dipole constant, μ_B is the Bohr magneton, $\hbar$ is the Plank constant, and the quantities g_S and g_I represent the electron-spin and nuclear "g factors," respectively. **S** denotes the electron-spin angular momentum, and **I** denotes the total nuclear angular momentum. For the TE_{011} mode of the cavity, the total magnetic field in the z direction can be expressed as [26]

$$\mathbf{B} = \left[B_0 + B_{\mathrm{MW}}J_0\left(3.832\frac{r}{R}\right)\sin\frac{\pi z}{L}\cos\omega t\right]\mathbf{e_z}, \tag{3}$$

where B_0 and B_{MW} are the biased magnetic field and the microwave magnetic field, respectively. r is the vertical distance from the cavity axis (the waist radius of the probe beam is about 3 mm). R and L represent the inner radius and height of the cavity, respectively. We assume that the magnetic field is uniform within the detection region in the radius direction (vertical to the axis) and neglect the microwave pumping effect on the cold atoms outside the detection region. Thus the magnetic field can be

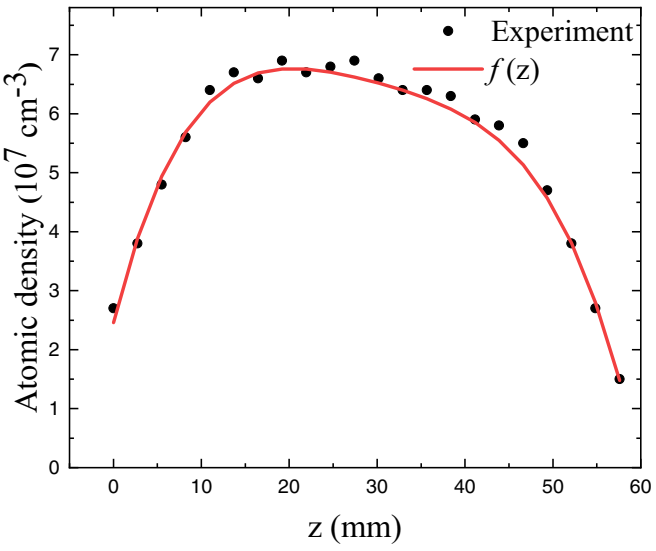

FIG. 3. The fitted experimental results of the atomic density distribution along the axis of the cavity.

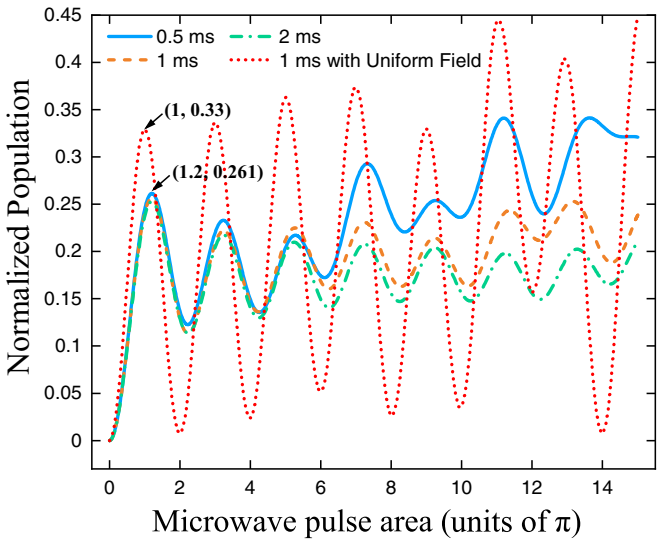

FIG. 4. The sum of atomic populations in the $|2, j\rangle$ $(j = 0, \pm 1)$ states. The blue curve, dashed orange curve, and dash-dotted green curve represent durations of 0.5, 1, and 2 ms, respectively. The dotted red curve represents the atoms in the uniform microwave field.

represented by

$$\mathbf{B} = \begin{cases} \left(B_0 + B_{\mathrm{MW}} \sin \frac{\pi z}{L} \cos \omega t\right)\mathbf{e_z} & 0 \leqslant r \leqslant 3 \text{ mm} \\ 0 & r > 3 \text{ mm}. \end{cases} \tag{4}$$

With weak magnetic fields and the rotating wave approximation, the Hamiltonian H_{rwa} of this six-level system represented with the basis vector $|F, m_F\rangle$ ($|2, 1\rangle$, $|2, 0\rangle$, $|2, -1\rangle$, $|1, 1\rangle$, $|1, 0\rangle$, $|1, -1\rangle$) can be written as

$$H_{\mathrm{rwa}} = \hbar \begin{pmatrix} \frac{\Omega_L}{2} & 0 & 0 & \frac{\sqrt{3}\Omega_B}{4} & 0 & 0 \\ 0 & 0 & 0 & 0 & \frac{\Omega_B}{2} & 0 \\ 0 & 0 & -\frac{\Omega_L}{2} & 0 & 0 & \frac{\sqrt{3}\Omega_B}{4} \\ \frac{\sqrt{3}\Omega_B}{4} & 0 & 0 & \Delta - \frac{\Omega_L}{2} & 0 & 0 \\ 0 & \frac{\Omega_B}{2} & 0 & 0 & \Delta & 0 \\ 0 & 0 & \frac{\sqrt{3}\Omega_B}{4} & 0 & 0 & \Delta + \frac{\Omega_L}{2} \end{pmatrix}, \tag{5}$$

where $\Delta = \omega - 2\mathrm{A}_{\mathrm{hfs}}/\hbar$ is the frequency detuning between the microwave field and the hyperfine ground states and $\Omega_B = \mu_B B_{\mathrm{MW}}/\hbar$ and $\Omega_L = \mu_B B_0/\hbar$ are the Larmor frequencies of the microwave and the biased magnetic field, respectively. Since the microwave field is nonuniform on the axis of the microwave cavity, we define the $\Omega_B\tau$ experienced by the atoms at the center point of the microwave cavity as the microwave pulse region. The experimental measured atomic density distribution on the axis of the cavity according to Ref. [27] is shown in Fig. 3. By fitting the atomic density data, we obtain a polynomial function $f(z)$, which is written as

$$f(z) = 2.46 + 0.596z - 0.0295z^2 + 6.31 \times 10^{-4}z^3 - 5.26 \times 10^{-6}z^4. \tag{6}$$

After the cooling phase, the microwave cavity can be seen as a gas chamber full of cold atoms, and the motion of cold atoms needs to be considered. The cold atoms with a distribution function of $f(z)$ experience different amplitudes and phases of the microwave field in different places along the axis. The evolution of the system can be described by the Liouville equation

$$\dot{\rho} = -\frac{\mathrm{i}}{\hbar}[H_{\mathrm{rwa}}, \rho] - \frac{1}{2}\{\Gamma, \rho\} + \Lambda, \tag{7}$$

where Γ is the relaxation matrix, which is mainly caused by the motion of atoms in the radial direction of the microwave cavity going beyond the detection region. Λ is the repopulation matrix, which describes the motion of atoms from outside into the detection region. The contribution of gravity and the decay of the coherence terms are relatively small since the interval between the cold-atom preparation and detection is only several milliseconds. Thus we assume that the atomic number in the detection region is conserved. According to Eq. (4), the atoms moving into the detection region from outside are evenly populated in the sublevel states $|F = 1, m_F = 0, \pm 1\rangle$. In the same basis vector $|F, m_F\rangle$, Γ and Λ can be written as

$$\Gamma = \begin{pmatrix} \gamma & 0 & 0 & 0 & 0 & 0 \\ 0 & \gamma & 0 & 0 & 0 & 0 \\ 0 & 0 & \gamma & 0 & 0 & 0 \\ 0 & 0 & 0 & \gamma & 0 & 0 \\ 0 & 0 & 0 & 0 & \gamma & 0 \\ 0 & 0 & 0 & 0 & 0 & \gamma \end{pmatrix},$$

$$\Lambda = \begin{pmatrix} 0 & 0 & 0 & 0 & 0 & 0 \\ 0 & 0 & 0 & 0 & 0 & 0 \\ 0 & 0 & 0 & 0 & 0 & 0 \\ 0 & 0 & 0 & \gamma/3 & 0 & 0 \\ 0 & 0 & 0 & 0 & \gamma/3 & 0 \\ 0 & 0 & 0 & 0 & 0 & \gamma/3 \end{pmatrix}, \tag{8}$$

where γ is the transit rate, which is obtained by fitting the probe light absorption of cold atoms, approximately 25 Hz [28,29]. All the atoms within the probe laser beam can be detected, so the average probability of cold atoms staying in the state $|i, j\rangle$ can be normalized as

$$\tilde{\rho}_{i,j} = \frac{\int_0^L \rho_{i,j}(z) f(z) dz}{\int_0^L f(z) dz}, \tag{9}$$

where $\rho_{i,j}(z)$ is the probability of an atom staying in the state $|i, j\rangle$ at position z and L is the inner height of the cavity, which is approximately 57.6 mm.

III. EXPERIMENTAL AND THEORETICAL RESULTS

In the experiment, we fixed the microwave pulse duration and increased the microwave power linearly cycle by cycle (microwave power is constant in a single cycle) to increase the microwave pulse area. According to Eq. (9), the population probability of all the atoms in $|F = 2\rangle$ can be calculated when the ^{87}Rb atoms are coherently driven by a resonant microwave field (biased magnetic field $B_0 = 0.63$ μT), and the results are shown in Fig. 4, in which the population probability curves for three microwave pulse durations, 0.5, 1, and 2 ms. are presented and oscillating in different ways for large pulse area.

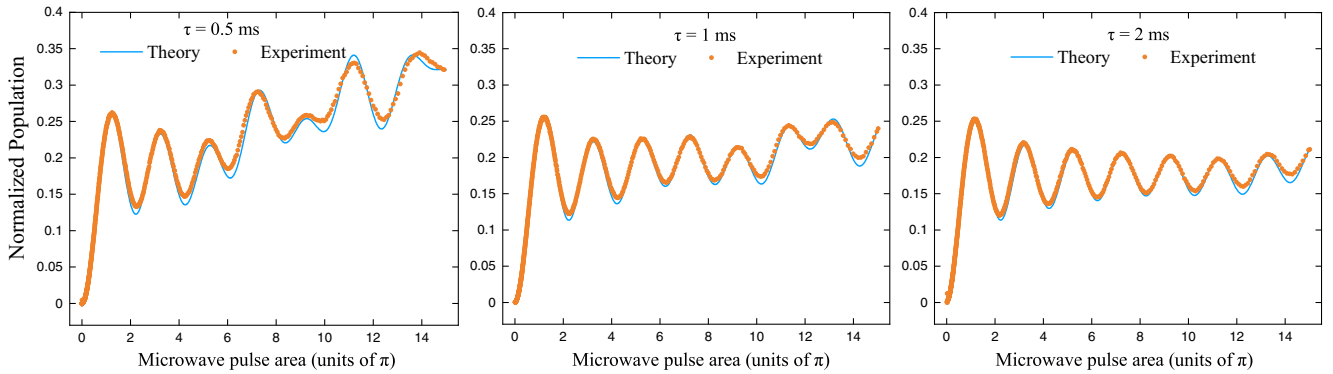

FIG. 5. The sum of atomic populations in the $|2, j\rangle$ ($j = 0, \pm 1$) states for different microwave durations. (a), (b), and (c) correspond to $\tau = 0.5$, 1, and 2 ms. The blue curve illustrates the theoretical calculation, and the orange dots represent the experimental measurements.

In addition, the sum of atoms in the $|2, j\rangle$ ($j = 0, \pm 1$) states with a uniform magnetic field is also shown for comparison. When $\tau = 0.5$ ms, the first-oscillation-maximum population of 0.26 and pulse area of 1.2π (which should be 0.33 and π in the ideal situation) are presented. Furthermore, the oscillations are distorted more seriously for the larger pulse area and the shorter microwave pulse duration.

The atom population after microwave Rabi interrogation was detected at a fixed time (about 4 ms after the cooling phase) for each cycle period, and we got one data point at each cycle; then the Rabi oscillation curve was obtained by scanning the microwave pulse area (changing a step at each cycle). We performed the corresponding experiments and normalized the population using Eq. (1), as shown in Fig. 5, which clearly exhibits the distortion of the Rabi oscillation. The microwave power is controlled by a microwave attenuator with a resolution of 0.03 dB. Since Ω_B is proportional to the eigenvector of the TE_{011} cavity mode, the relationship between the attenuation value P (units of decibels) and Ω_B can be expressed as

$$\frac{P + C}{D} = \log_{10} \Omega_B, \tag{10}$$

where P is controlled by the attenuator and the value of Ω_B is determined by the theoretical calculation; thus the constants $C = 21.9$ and $D = 18.7$ can be determined by fitting the first and second peaks of the experimental Rabi oscillations. Then, we can use Eq. (10) to calibrate the microwave pulse area for any attenuation values. The experimental results agree with the theoretical calculations, except in the region of large pulse area. A possible reason is that the function $f(z)$ does not perfectly describe the actual atom density distribution inside the microwave cavity and we ignored the inhomogeneity of the microwave magnetic field in the radial direction. Compared with the Rabi oscillations in a uniform microwave magnetic field, the collapse of the Rabi oscillations and the shift of the maximum oscillation position are due to the inhomogeneity of the microwave magnetic field and atom distribution. Therefore we can estimate the inhomogeneity of the microwave magnetic field by measuring the Rabi oscillations.

In order to explain the phenomenon of Rabi oscillation distortion, we calculated three Rabi oscillations between hyperfine sublevel transitions and show the results in Fig. 6. The three probabilities of transition are denoted as $\tilde{\rho}_{2,0}$, $\tilde{\rho}_{2,1}$, and $\tilde{\rho}_{2,-1}$, and the probability $\sum_j \tilde{\rho}_{2,j}$ is equal to the sum of $\tilde{\rho}_{2,0}$, $\tilde{\rho}_{2,1}$, and $\tilde{\rho}_{2,-1}$. It can be seen that $\sum_j \tilde{\rho}_{2,j}$ is abnormal. Therefore we can conclude that the distortion of the Rabi oscillations is caused by the π transitions between magnetically sensitive sublevels, which could also cause Rabi pulling [30].

The above results show that atoms on the magnetically sensitive Zeeman sublevels will affect the performance of the atomic clock. The probability of magnetically sensitive transitions ($|1, 1\rangle \rightarrow |2, 1\rangle$ and $|1, -1\rangle \rightarrow |2, -1\rangle$) is increased by increasing the microwave power, and then the Rabi oscillations become distorted. The best way to resolve this problem is to pump all atoms to the clock state $|2, 0\rangle$ and design a new microwave cavity with a uniform magnetic field. However, this is difficult to realize with the present setup, and changes to the setup are needed. For the present system, we can reduce these magnetically sensitive transitions by selecting the appropriate amplitude of the biased magnetic field.

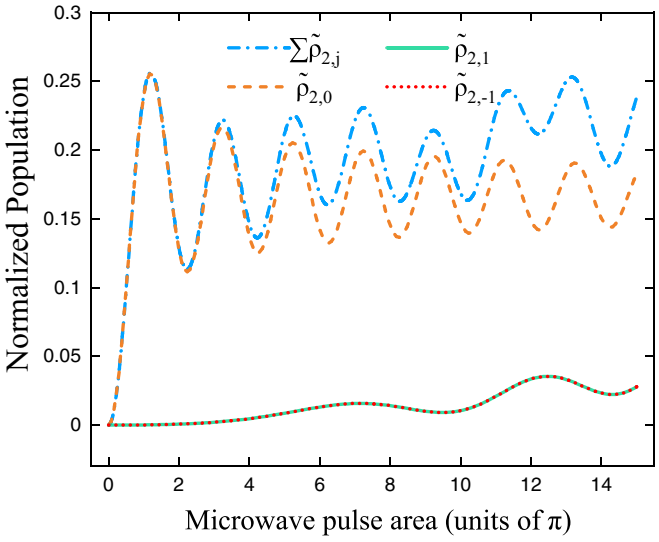

FIG. 6. Rabi oscillations between Zeeman sublevels of $|1, 0\rangle \rightarrow |2, 0\rangle$ (dashed orange curve), $|1, 1\rangle \rightarrow |2, 1\rangle$ (green curve), and $|1, -1\rangle \rightarrow |2, -1\rangle$ (dotted red curve) at $\tau = 1$ ms, and their sum (dash-dotted blue curve).

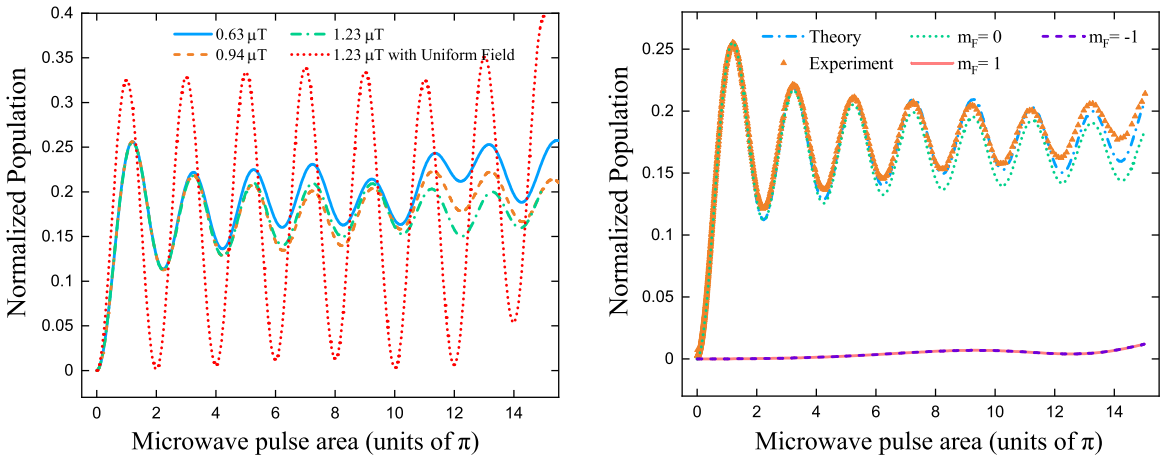

FIG. 7. (a) The sum of atomic populations in the $|2, j\rangle$ ($j = 0, \pm 1$) states for different biased magnetic fields ($\tau = 1$ ms). The blue curve, dashed orange curve, and dash-dotted green curve represent the oscillation magnitudes under a biased magnetic field of $B_0 = 0.63$, 0.94, and 1.23 μT, respectively. The dotted red curve represents the atoms in the uniform microwave magnetic field. (b) Probability of different sublevels ($\tau = 1$ ms, $B_0 = 1.23$ μT). The orange triangles represent the experimental measurements.

Figure 7(a) shows the calculation results of Rabi oscillations at different biased magnetic fields when $\tau = 1$ ms. The shape of the Rabi oscillations approaches normal when the biased magnetic field increases. When the biased magnetic field $B_0 = 1.23$ μT and pulse duration $\tau = 1$ ms, the Rabi oscillations are measured, and the three Rabi oscillations between the Zeeman sublevels are calculated for comparison, as shown in Fig. 7(b). The contribution of the magnetically sensitive sublevel transition is much smaller than the contribution in the case of $B_0 = 0.63$ μT and is very close to zero. These results are useful for improving the performance of the atomic clock and provide a suitable reference for designing a new system.

IV. CONCLUSION

In summary, we have investigated the Rabi oscillations of cold atoms in the ISCAC, and the experimental measurements and theoretical analysis of the clock-state Rabi oscillation distortion are demonstrated. The distortion of Rabi oscillations is caused by the nonuniform microwave magnetic field and the inhomogeneous distribution of the cold atoms inside the microwave cavity. The magnetically sensitive transitions between hyperfine Zeeman sublevels were the primary contributors. These results help us to understand the limitations of the present setup and provide useful guidance for further improving the performance of the compact cold-atom clock, which can be extended to types of atomic clocks using a microwave cavity.

ACKNOWLEDGMENT

This work was supported by National Natural Science Foundation of China (Grants No. 61727821 and No. 61875215).

[1] I. Rabi, Phys. Rev. **51**, 652 (1937).
[2] M. Brune, F. Schmidt-Kaler, A. Maali, J. Dreyer, E. Hagley, J. M. Raimond, and S. Haroche, Phys. Rev. Lett. **76**, 1800 (1996).
[3] L. Horstman, N. Hsu, J. Hendrie, D. Smith, and J. C. Diels, Photonics Res. **8**, 252 (2020).
[4] F. Assemat, D. Grosso, A. Signoles, A. Facon, I. Dotsenko, S. Haroche, J. M. Raimond, M. Brune, and S. Gleyzes, Phys. Rev. Lett. **123**, 143605 (2019).
[5] S. Blatt, J. W. Thomsen, G. K. Campbell, A. D. Ludlow, M. D. Swallows, M. J. Martin, M. M. Boyd, and J. Ye, Phys. Rev. A **80**, 052703 (2009).
[6] S. Peil, J. L. Hanssen, T. B. Swanson, J. Taylor, and C. R. Ekstrom, Metrologia **51**, 263 (2014).
[7] Y. Ovchinnikov and G. Marra, Metrologia **48**, 87 (2011).
[8] T. P. Heavner, E. A. Donley, F. Levi, G. Costanzo, T. E. Parker, J. H. Shirley, N. Ashby, S. Barlow, and S. R. Jefferts, Metrologia **51**, 174 (2014).
[9] T. H. Stievater, X. Li, D. G. Steel, D. Gammon, D. S. Katzer, D. Park, C. Piermarocchi, and L. J. Sham, Phys. Rev. Lett. **87**, 133603 (2001).
[10] B. Wang, X. Z. Zeng, and Z. Y. Li, Photonics Res. **8**, 343 (2020).
[11] J. M. Martinis, S. Nam, J. Aumentado, and C. Urbina, Phys. Rev. Lett. **89**, 117901 (2002).
[12] T. A. Johnson, E. Urban, T. Henage, L. Isenhower, D. D. Yavuz, T. G. Walker, and M. Saffman, Phys. Rev. Lett. **100**, 113003 (2008).
[13] S. Micalizio, C. E. Calosso, A. Godone, and F. Levi, Metrologia **49**, 425 (2012).
[14] A. Clairon, C. Salomon, S. Guellati, and W. D. Phillips, Europhys. Lett. **16**, 165 (1991).
[15] H. S. Kang, Y. G. Kim, H. Y. Jung, C. H. Oh, P. S. Kim, and H. S. Lee, IEEE Trans. Instrum. Meas. **50**, 1787 (2001).
[16] S. R. Jefferts, J. H. Shirley, N. Ashby, E. A. Burt, and G. J. Dick, IEEE Trans. Ultrason., Ferroelectr., Freq. Control **52**, 2314 (2005).

[17] P. Liu, Y.-L. Meng, J.-Y. Wan, X.-M. Wang, Y.-N. Wang, L. Xiao, H.-D. Cheng, and L. Liu, Phys. Rev. A **92**, 062101 (2015).
[18] F. X. Esnault, N. Rossetto, D. Holleville, J. Delporte, and N. Dimarcq, Adv. Space Res. **47**, 854 (2011).
[19] S. Tremine, E. de Clercq, and P. Verkerk, Phys. Rev. A **96**, 023411 (2017).
[20] W. Ketterle, A. Martin, M. A. Joffe, and D. E. Pritchard, Phys. Rev. Lett. **69**, 2483 (1992).
[21] E. Guillot, P. E. Pottie, and M. Dimarcq, Opt. Lett. **26**, 1639 (2001).
[22] M. Langlois, L. De Sarlo, D. Holleville, N. Dimarcq, J. F. Schaff, and S. Bernon, Phys. Rev. Appl. **10**, 064007 (2018).
[23] F. X. Esnault, D. Holleville, N. Rossetto, S. Guerandel, and N. Dimarcq, Phys. Rev. A **82**, 033436 (2010).
[24] X. Wang, Y. Sun, H.-D. Cheng, J.-Y. Wan, Y.-L. Meng, L. Xiao, and L. Liu, Phys. Rev. Appl. **14**, 024030 (2020).
[25] G. D. Mcdonald, Detecting atomic shot noise on ultra-cold atom clouds, Bachelor's honors thesis, Australian National University, 2009.
[26] F. Riehle, *Frequency Standards: Basics and Applications* (Wiley-VCH, Weinheim, 2005), p. 96.
[27] Y.-L. Meng, H.-D. Cheng, B.-C. Zheng, X.-C. Wang, L. Xiao, and L. Liu, Chin. Phys. Lett. **30**, 063701 (2013).
[28] W.-Z. Zhang, X.-C. Wang, H.-D. Cheng, L. Xiao, L. Liu, and Y.-Z. Wang, Chin. Phys. Lett. **26**, 083703 (2009).
[29] X.-C. Wang, H.-D. Cheng, and L. Liu, Chin. Opt. Lett. **10**, 100201 (2012).
[30] S. Micalizio and A. Godone, Phys. Rev. A **99**, 043425 (2019).